Geomorphological landslide inventory map of the Daunia Apennines, southern Italy

Francesca Ardizzone[1], **Francesco Bucci**[1], **Mauro Cardinali**[1], **Federica Fiorucci**[1], **Luca Pisano**[2], **Michele Santangelo**[1], **and Veronica Zumpano**[2]

[1]CNR – IRPI, Via della Madonna Alta 126, 06128, Perugia, Italy
[2]CNR – IRPI, Via Amendola 122, 70126, Bari, Italy

Correspondence: Mauro Cardinali (mauro.cardinali@irpi.cnr.it)

Abstract. Detailed and accurate geomorphological historical landslide inventory maps are an invaluable source of information for many research topics and applications. Their systematic preparation worldwide has been advised by many researchers as it may foster our knowledge on landslides, their spatial and temporal distribution, their potential interaction with the built environment, their contribution to landscape dynamics, and their response to climate change in the past. Due to the extreme variability of the morphological and radiometric elements that can reveal historical landslides, geomorphological historical landslide inventory maps are produced by expert interpretation, which makes it a time-consuming and expensive process, which often discourages wide-area mapping activities. In this paper we present a new geomorphological historical landslide inventory map for a 1460 km^2 area in the Daunia Apennines, the north-western sector of the Apulia (Puglia) region, in southern Italy. The inventory contains 17 437 landslides classified according to relative age, type of movement, and estimated depth. Landslides were mapped according to rigorous and reproducible criteria applied by two teams of expert photo interpreters to two sets of stereoscopic aerial photographs taken in 1954/55 and 2003. The dataset consists of a digital archive publicly available at https://doi.org/10.1594/PANGAEA.942427 (Cardinali et al., 2022).

1 Introduction

Landslides are widespread natural hazards that occur worldwide, posing threats to populations, structures and infrastructures and causing relevant economic damage to society (Donnini et al., 2017; Froude and Petley, 2018; Petley, 2012). Availability of information on landslide locations, types, and sizes is key basic information for many activities, from research to emergency support and land planning. Nevertheless, expert landslide mapping is not an investment priority in many countries and institutions, and hence homogeneous wide-scale landslide maps are rare (Guzzetti et al., 2012; Bucci et al., 2021), although the availability of a landslide inventory map is fundamental to the production of landslide hazard and risk maps (Thiery et al., 2020). As a result, several applications spanning from land management to susceptibility modelling that would benefit from more homogeneous

and complete datasets rely on often poor or incomplete/inconsistent data.

Any landslide mapping activity assumes (i) that landslides leave discernible features on the territory, i.e. a "landslide signature" made by radiometric and morphologic elements (Fiorucci et al., 2018; Guzzetti et al., 2012; Santangelo et al., 2022), (ii) that, in the case of use of remote sensing, the data used (e.g. images) portray them, (iii) that the technique adopted is adequate to the data used, and (iv) that the operator (or the automatic or semi-automatic classification system) is able to exploit those features to detect and map landslides. Therefore, any landslide mapping activity is affected by a degree of incompleteness and inconsistency that stems from these basic assumptions. Landslides can remain unnoticed since (i) features may be cancelled by erosion, other landslides, and/or human activity (Malamud et al., 2004), (ii) the type of image or its spectral and spatial resolution

may be inadequate for some types or sizes of landslides or for some locations (e.g. slope orientation), and (iii) interpreters or (semi-)automatic systems may be unable to map some landslides using certain images or techniques (e.g. lack of experience, poor or incorrect system training).

Landslide inventory maps (LIMs) are the simplest tools to represent landslide distribution in a territory. They usually display landslide locations preferably as polygons rather than points or lines, which should be used only for scale representation issues. LIMs usually store landslide attributes such as type of movement, estimated time of occurrence, estimated depth, activity at the date of the observation if available, and other more detailed data depending on availability and on the scale of the work (Bucci et al., 2021; Guzzetti et al., 2012; Santangelo et al., 2015).

Different types of inventories can be prepared. Event inventories (E-LIMs, Antonini et al., 2002; Ardizzone et al., 2012; Donnini et al., 2017; Fiorucci et al., 2018; Harp and Jibson, 2017; Mondini et al., 2012; Santangelo et al., 2022) report landslides that were triggered by specific events (i.e. rainfall, rapid snowmelt, volcanic eruption, earthquake). Geomorphological inventories (G-LIMs) report landslides that can be recognised by geomorphologists, usually from the expert interpretation of stereoscopic aerial photographs (Bucci et al., 2021; Cardinali et al., 2001; Guzzetti et al., 2012; Santangelo et al., 2015), but lidar-derived images are also widely used (Niculiță et al., 2016; Razak et al., 2013; Schulz, 2004; Van Den Eeckhaut et al., 2007). They can be seen as the result of many landslide events over thousands of years (Malamud et al., 2004). Multi-temporal landslide inventories (M-LIMs) include the information of G-LIMs and also report landslides that occurred in the last tens of years as visible on historical images available at (possibly) regular time steps of several years (Galli et al., 2008; Guzzetti et al., 2012; Zumpano et al., 2020).

G-LIMs can be prepared for wide areas and provide a fundamental source of information about landslides that occurred in the last tens of thousands of years. This particular type of inventory is an invaluable source of data but is time-consuming and requires a high level of training and experience to get accurate and reliable results (Guzzetti et al., 2012), which usually hampers the systematic preparation of G-LIMs at regional or even national/continent scales.

This paper presents a new G-LIM prepared for the Daunia mountains in the Apulia (Puglia) region, southern Italy. For this area, historically affected by diffuse slow-moving large landslides, the regional government required the preparation of a new landslide inventory to overcome the inhomogeneity among the existing inventories in terms of the spatial distribution of landslides and of techniques adopted and working and publication scales. The landslide inventory map was produced through the interpretation of two sets of stereoscopic aerial photographs, taken in 1954/55 and 2003, supplemented by targeted field checks. The new landslide inventory is an entirely original dataset openly accessible at https://doi.org/10.1594/PANGAEA.942427 (Cardinali et al., 2022).

2 Study area

The study area extends for $1460\,\mathrm{km^2}$ in the northern-western sector of the Apulia (Puglia in Italian) region (southern Italy) (Fig. 1). The area corresponds to the Daunia Apennines, located in the external (i.e. eastern) part of the southern Apennine fold and thrust belt system.

The southern Apennines are the result of compressive tectonic dynamics characterised by an oblique collision of the Calabrian forearc with the Apulian margin (Filice and Seeber, 2019) that evolved from an antecedent subductive phase of thrust emplacement (Vitale et al., 2011; Vitale and Ciarcia, 2013). Currently, the external (eastern) margin preserves the compressive tectonics, while the internal sector is characterised by an extensive dynamic with tension faults that dissect the pre-existent fold and thrust structure (Brozzetti et al., 2009; Schiattarella et al., 2003).

The western sector of the Daunia Apennines is characterised by a wide variety of formations, mainly clay-rich flysch lithologies with different mechanical properties highly affected by folds and faults (Cotecchia et al., 2020; Losacco et al., 2021; Pellicani et al., 2014b), resulting in medium to high relief, with the elevations ranging between 55 and 1152 m a.s.l., where the highest peak is represented by Monte Cornacchia. Morphologically, it is strongly influenced by both the prolonged tectonic stresses and by the differences in composition and erodibility, where selective erosion has alternatively produced gentler and rounded slopes on the more erodible clayey formations and steep slopes cut on harder rocks. In this sector, the orography associated with the widespread presence of clay-rich materials and the intense deformation is the main cause of landslides (Ciarcia et al., 2003; Losacco et al., 2021; Spalluto et al., 2021; Wasowski et al., 2010; Zumpano et al., 2020). The eastern sector is characterised by the sub-Apennine clay formation and alluvial deposits and by gentle slopes slightly dipping towards the north-east. In this sector, several orders of terraced fluvial deposits overlay the sub-Apennine clay formation. Here, mass movements are mainly concentrated along the scarps of the terraces.

The Daunia Apennines are influenced by a Mediterranean sub-humid climate with mild and often wet winters and usually hot and dry summers. In general, inter-annual temperature variations are significant and the total yearly precipitation seldom exceeds 1000 mm (Wasowski et al., 2012, 2010). In the area, torrential streams flow NE–SW, draining the sediments from the Daunia Apennines through the Tavoliere plain towards the Adriatic Sea.

In response to the lithostructural and morphoclimatic setting of this area, landslides are widespread. They are mostly slow-moving slide-type and flow-type movements, involving
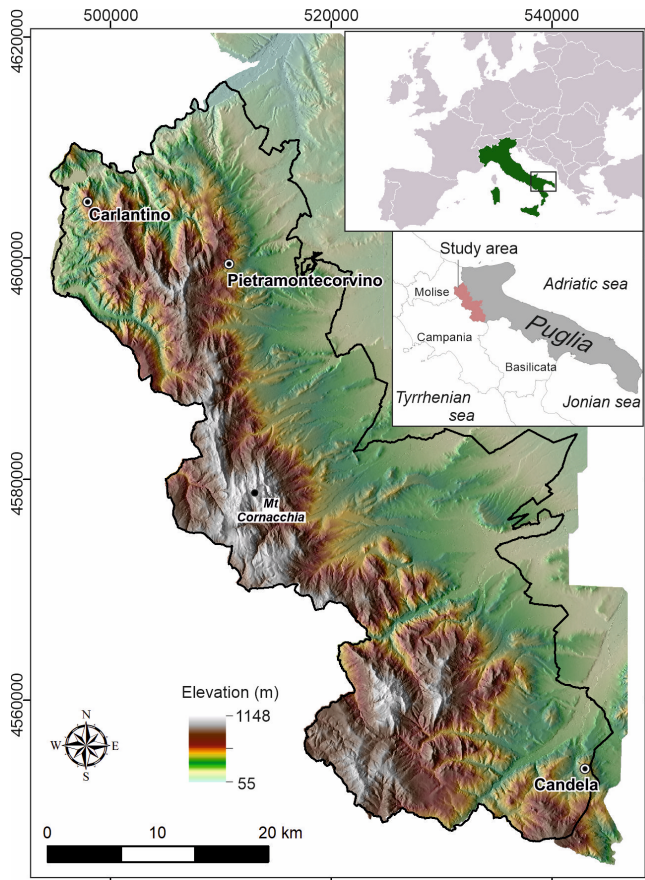
Figure 1. Location map of the study area. Base map: digital terrain model (DTM) at 8 m resolution made available by the Regione Puglia administration.

soil and earth, and secondarily rock material. Rapid-moving (i.e. debris flows) and fast-moving (i.e. rockfalls) landslides are less abundant (Wasowski et al., 2010, 2012; di Lernia et al., 2022; Zumpano et al., 2020). The widespread presence of landslides in the area is a major cause of damage to urban settlements, to the road network, and to the stability of buildings. These features determine a direct effect on the development and the economy of the area (Pellicani et al., 2014b, a; Zumpano et al., 2020).

3   Materials and methods

The procedure adopted to prepare the landslide inventory map is illustrated in Fig. 2. The overall procedure consists of three main phases: (i) data collection, (ii) photo interpretation, and (iii) editing. The entire work was carried out by a "mapping team" made up of four interpreters and one supervisor and an "editing team" made up of three GIS editors.

The first stage of the work consisted in the collection of data available for the study area (i.e. ancillary data, Fig. 2; complete list in Appendix A) and the pre-processing of the

aerial photographs to produce oriented stereo-models in absolute coordinates to be used for the visual interpretation in a photogrammetric GIS environment. Such photogrammetric pre-processing included the interior and exterior orientations of each pair of aerial photographs. For the interior orientation, a non-metric camera model was adopted for which the focal length of the camera, the flight altitude, and the pixel size were required, while for the representation of the ground-to-image geometry (exterior orientation), ground control points (GCPs) were used. The planimetric coordinates (x, y) of GCPs were manually chosen by visual comparison of the aerial photographs and an orthophoto available taken in 2006 (at 1 m resolution available for download at https://www.sit.puglia.it/, last access: 6 February 2023) and 1988 (at 1 m resolution, available as a Web Map Service at http://www.pcn.minambiente.it/mattm/servizio-wms/, last access: 6 February 2023). The altimetric coordinate (z) of the GCPs was obtained from a digital elevation model (8 m resolution available for download at https://www.sit.puglia.it/). Stereo models were prepared for both aerial photograph epochs, 1954/55 and 2003, i.e. the oldest and the latest aerial photograph acquisitions available for the entire study area.

The second phase of the work is the photo interpretation (Fig. 2) of the aerial photographs. At the very initial stage of the work, the entire mapping team defined a legend through an expeditious photo interpretation in representative geomorphological settings and according to well-established landslide classification schemes (Cruden and Varnes, 1996; Hungr et al., 2014; WP/WLI, 1993). Then, divided into pairs, for each stereo-pair the mapping team prepared a preliminary interpretation (first-level G-LIM in Fig. 2) that was then reviewed by the supervisor and discussed with the mapping team. After this step, an updated version of the map was produced (second-level G-LIM in Fig. 2). Each of the two mapping team pairs performed their preliminary photo interpretation in alternating strips along the flight plan. The side lap between subsequent strips was therefore common between the different pairs of interpreters, and it was used to compare, correct, and homogenise the interpretation made by different sub-teams independently. Such a continuous interaction among geomorphologists made it possible to best define the characteristics of the identified landslides, limiting interpretation inconsistencies among operators. Finally, at significant advancement steps, extensive field checks were performed by the entire mapping team to check, validate, and correct the inventory based on field evidence. After the field check stage, the interpretation phase was concluded and the landslide mapping considered quasi-definitive; i.e. occasional changes might be needed if inconsistencies were observed at the third stage (e.g. consistency with contour maps and hydrography).

The third and last step of the procedure (editing) consists in the preparation of the geographical database. The interpreted features drawn as polylines by the mapping teams were verified on the digital topography, i.e. con-
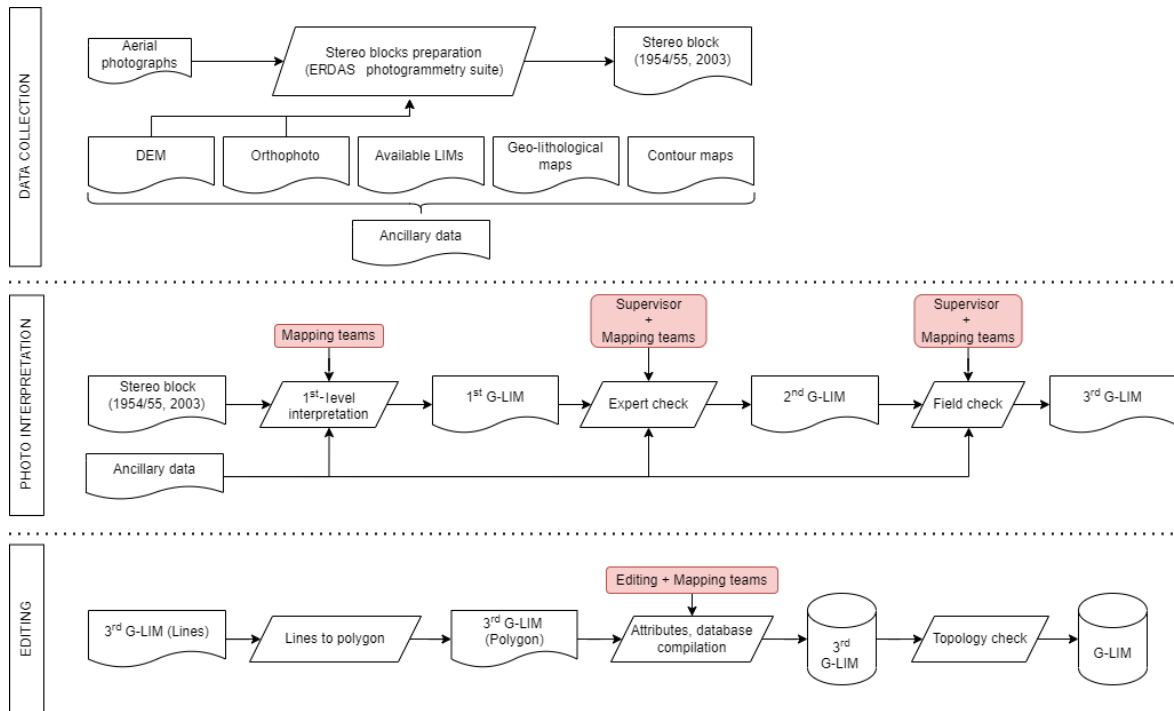
Figure 2. Flowchart of the procedure to prepare the geomorphological landslide inventory map. Pink rectangles indicate contributions of different teams/operators.

tour lines at scale 1 : 5000 (editing phase in Fig. 2). The checked polylines were then converted into polygon features and verified with topological checks to avoid overlapping. Finally, the polygons were coded according to the adopted legend (the legend description is available in Sect. 4 and the database schema is described in the metadata of the digital archive available at https://doi.org/10.1594/PANGAEA.942427, Cardinali et al., 2022). Landslides recognised in the study area were classified by type according to Cruden and Varnes (1996) and Hungr et al. (2014). Additionally, according to WP/WLI (1993), landslides were classified based on the estimated depth (as shallow or deep-seated) and the inferred relative age (as relict, very old, old, or recent). Examples and descriptions of landslides of different types, relative ages, and depths as well as of other geomorphological elements are detailed in Sect. 4. A more detailed explanation of the criteria used for the definition of the legend was given by Bucci et al. (2021).

3.1 Available data

The G-LIM of the Daunia Sub-Apennines was prepared through systematic visual interpretation of a set of 270 b/w stereoscopic aerial photographs taken in 1954/55 at 1 : 33 000 scale and of 384 b/w stereoscopic aerial photographs taken in 2003 at 1 : 30 000 scale. Aerial photographs were provided as

800 dpi scanned copies. All the ancillary data used for interpretation are listed and described in detail in Appendix A.

3.2 Hardware and software

For the interpretation phase we used the digital stereoscopic vision 3D PluraView System, composed of two monitors for the stereoscopic vision of digital images, and a 45° inclined mirror placed on the bisector of the two monitors equipped with passive 3D glasses (https://www.3d-pluraview.com/en/, last access: 6 February 2023). A dedicated computer, equipped with IMAGINE Photogrammetry software (https://www.hexagongeospatial.com/products/power-portfolio/imagine-photogrammetry, last access: 6 February 2023), was used for the pre-processing of digital stereoscopic images, and ArcGis software with the 3D Analyst extension tool was used to digitise the 3D data in a GIS environment (Ardizzone et al., 2013; Fiorucci et al., 2015). The spatial resolution of the images (~ 1 m for the 1954/55 epoch, ~ 0.9 m for the 2003 images) and the zoom capability of the 3D PluraView System allow the identification of very small features. The stereo pairs were investigated using a zoom level at scale 1 : 2500 to obtain mapped features compatible with a publication scale of 1 : 5000. The capabilities of the ERDAS IMAGINE™ Photogrammetry Suite and ArcGIS™ Stereo Analyst to prepare, manage, and view multiple sets of oriented images, all with the same reference

Table 1. Descriptive statistics of landslides by relative age.

	Number of features	Total area (m^2)	Minimum area (m^2)	Maximum area (m^2)
Very old relict landslides	37	8.85×10^7	1.38×10^5	6.78×10^6
Very old landslides	120	8.75×10^7	5.82×10^4	2.86×10^6
Pre-2003 landslides	14 793	3.39×10^8	7.1×10^1	2.3×10^6
Recent landslides (2003)	2049	5.01×10^6	1.89×10^1	1.63×10^5
Widespread landslides	348	1.13×10^7	3.78×10^2	3.54×10^5
Entire inventory	17 347	4.42×10^8	1.89×10^1	6.77×10^6

system, allowed the fast comparison of landscape features in different epochs, improving the interpretation.

4 Geomorphological landslide inventory map

The inventory covers an area of 1460 km^2 and includes 17 347 landslides (Fig. 3) corresponding to an average density of about 15.6 landslides per square kilometre (Table 1) if lowland plains are excluded. Locally, landslide density reaches 60 landslides per square kilometre. Landslide size (landslide area, A_L in square metres) is in the range $1.9 \times 10^1 < A_L < 6.8 \times 10^6$ (Table 1). Overall, landslides cover an area of 442 km^2, which represents the 39 % of the hilly and mountainous portion of the study area.

In this section the different groups of elements comprising the inventory will be analytically described. Section 4.1 to 4.3 describe landslides classified according to their relative age, type classification, and estimated depth. Section 4.4 describes the widespread landslides (i.e. landslides represented as groups of failures due to their small size and high spatial frequency). Section 4.5 gives the descriptive statistics of the landslide inventory, and Sect. 4.6 presents the geomorphological elements (i.e. elements that are considered in relation to slope evolution and that can provide useful information for landslide identification and mapping).

4.1 Landslide by relative age

Based on their appearance in aerial photographs, landslides were classified according to their relative age, namely (i) very old relict landslides, (ii) very old landslides, (iii) old landslides, and (iv) recent landslides (Fig. 3). The four relative age levels are the result of a major subdivision, referring to the general morphologic appearance of landslides (Keaton and DeGraff, 1996), and are based on the assumption that evidence of landslides becomes less obvious with increasing age, due, for example, to erosion processes, vegetation growth, and occurrence of other landslides. Hence, older landslides are more difficult to detect than more recent ones.

Landslide modifications within the two epochs (1954 and 2003) were negligible for very old relict and very old landslides, whereas they were more frequent for old landslides

(i.e. pre-2003). Therefore, the final landslide delineation considers by definition the latest evidence within the 49-year time interval.

In our G-LIM, the most represented landslides in the study area are old landslides (Table 1, Fig. 3c), corresponding to 14 793 landslides covering a total landslide area of 339 km^2. Recent landslides (Fig. 3d) are also very numerous (2049). They are generally small and cover a total area of 5 km^2. Very old relict and very old landslides (Fig. 3a, b) are represented by 37 and 120 landslides, respectively, and cover areas of 88 and 87 km^2. The feature of being fewer and larger than more recent landslides is common to other geomorphological inventories (Bucci et al., 2021, 2016a; Santangelo et al., 2015). The spatial relationships between landslides belonging to the relative age groups are displayed in Fig. 4, where a representative example of the landslide relative age pattern for the entire inventory is shown.

Figure 4b–e show the inventory disaggregated according to the four relative age classes recognised. The sequence of the four panels represents a timeline where landslides of each time step are shown with their own colour, the same as Fig. 4a, whereas landslides belonging to antecedent time steps are represented in white.

In addition to the four mentioned relative age classes, a generation principle based on crosscut relationships defines minor sub-divisions within each age class: younger landslides cover the older ones. For the overall inventory, this criterion allowed us to detect up to (i) two landslide generations within the relict landslides, (ii) two generations within the very old landslides, (iii) four generations within the old landslides, and (iv) two generations within the recent landslides. Such minor sub-divisions are applicable only to landslides that overlap; i.e. they are not applicable to landslides that do not overlap. For instance, in Fig. 4d the age class "old" records up to three overlapping classes, indicated, respectively, in light orange (first failure "old"), orange (second failure "old"), and red (third failure "old").

Landslides classified as very old relict (Fig. 4b) generally affect entire slopes, where the energy of the relief is greatest. They are usually controlled by the geological and lithological structure and the presence of main faults (Bucci et al., 2016a). Very old relict landslides are deeply dismantled by
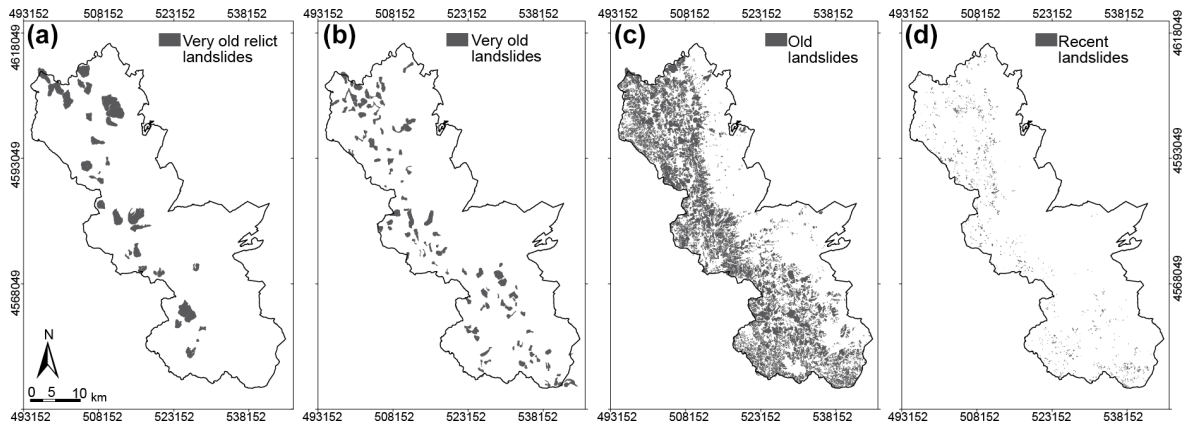
Figure 3. Spatial distribution of (a) very old relict landslides, (b) very old landslides, (c) old landslides and (d) recent landslides.
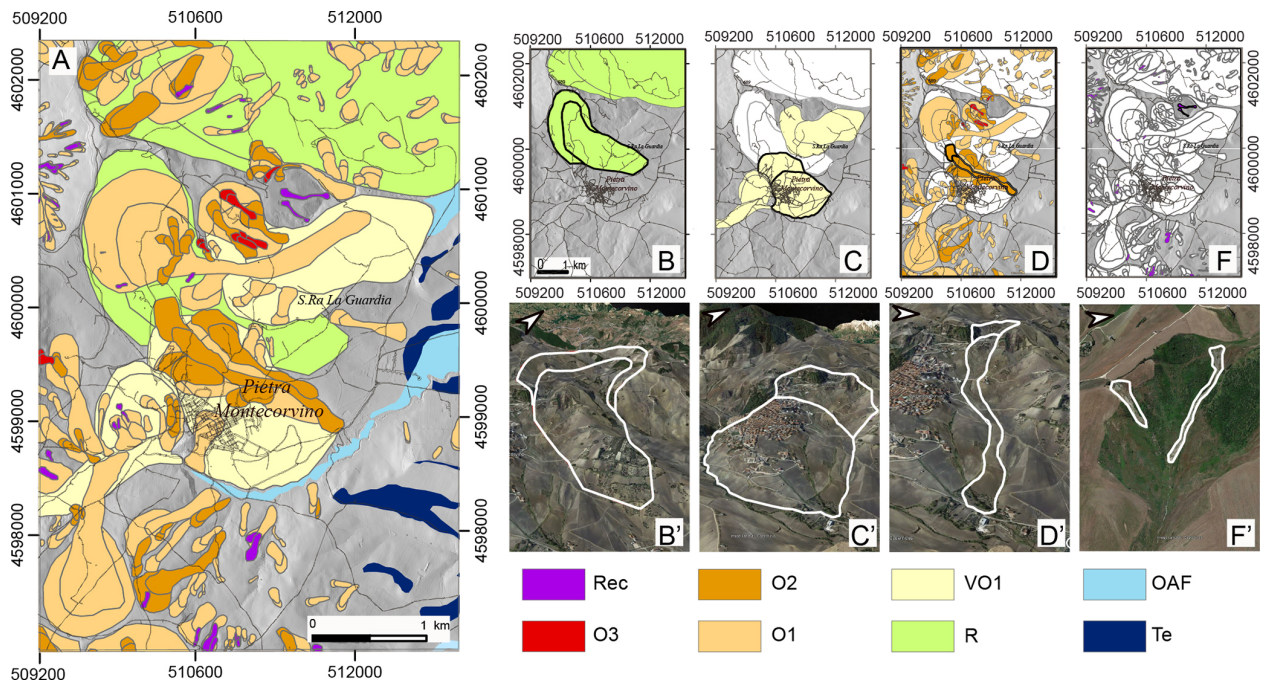

Figure 4. Examples of the relative age classes in the area of the Pietramontecorvino municipality (see Fig. 1 for reference). **(a)** Detail of the inventory in the selected location. The black-outlined polygon indicates the area in B to I. Very old relict landslides **(b)**, very old landslides **(c)**, old landslides **(d)** and recent landslides **(e)** are portrayed in detail. Black-outlined polygons in B to E are represented singularly in a perspective view on © GoogleEarth™ in B′ to F′. In the legend: Rec: recent landslides; O1, O2, O3: old landslides of first, second, and third generation; VO1: very old landslides of first generation; R: relict landslides; OAF: old alluvial fan; Te: terrace.

the erosive action of water courses and often reshaped by recurring gravitational phenomena. These morphological modifications are often related to the regional morphological and tectonic evolution, which has determined considerable base-level variations in the study area. As a consequence, these landslides are often suspended with respect to the present-day base level and are totally or partially isolated from the recent evolution of the drainage network. Therefore, very old relict landslides are considered to have occurred under ge-

omorphological and climatic conditions different from the present day (WP/WLI, 1993).

Landslides classified as very old (Fig. 4c) show evidence of active and passive interaction with river dynamics, being often partly eroded from them and locally modifying their path. Also, morphological modifications of very old landslides can be induced by the occurrence of other mass movements over time. Very old landslides are generally large and in agreement with the present-day river network: they are mainly distributed where the local relief is high, and they

often occur in or near very old relict landslides as local reactivations.

Landslides classified as old (Fig. 4d) present recognisable evidence on both the 1954/55 and 2003 aerial photograph epochs. These landslides generally present morphological characteristics typical of landslides which are not modified by erosion (e.g. concave–convex shape of the slope, presence of steps, and back slopes in the deposit area). Old landslides tend to cluster spatially, as is evident from the several generations of mass movements that were recognised. Spatial clustering of old landslides is even more evident in the vicinity of very old or very old relict landslides. Old landslides are hypothesised to have occurred in more recent times (as yet undefined) compared to very old and very old relict landslides.

Landslides classified as recent (Fig. 4e) are represented by landslides that show evidence of having occurred close to the date of the 2003 aerial image. The diagnostic elements for the identification of recent landslides refer not only to the morphological evidence, but above all to the spectral elements (photographic tone and contrast), which can be perceived even with a bi-dimensional (2D) view of the images. Recent landslides are mainly shallow failures essentially involving the soil horizons or the alteration of the debris cover for a few metres in depth. Their spatial distribution is ubiquitous and only limited to the areas where the triggering event induced the landslides. Therefore, they were found both in previously unaffected slopes or within pre-existing landslides.

As opposed to the recent landslides, whose evidence is stronger, some uncertainty characterises the delineation of older landslide borders, whose boundaries can be affected or even dismantled by different degrees of erosion or covered by more recent slope failures. General considerations on the relative age criteria of classification (Keaton and DeGraff, 1996) support our own experimental observations on landslide morphological appearance that the uncertainty degrees in landslide mapping increase with the increasing landslide age (Bucci et al., 2021). However, we do not have information on the absolute ages of the landslides in our study area and only hypothesise that the majority of the mapped landslides occurred in the last 10–20 Kyr, as suggested by findings of recent studies on landslide age in the southern Apennines (Gioia et al., 2011) and elsewhere (Niculiță et al., 2016; Pánek et al., 2014).

4.2 Landslide by type

The types of landslides are assigned based on the morphological and radiometric signatures of each landslide on the aerial photographs. Landslide types included in the legend of the G-LIM are (i) slide-type landslides (which include deep-seated rock slides or earth slides, shallow soil slides, or earth slides), (ii) earth flow, (iii) slide-earth flow, (iv) debris flow, (v) rockfall, and (vi) sackung (Table 2). In Table 2, widespread landslides refer to polygons representing groups of landslides whose size is smaller than the smallest feature that can be represented at the publication scale of the final map.

According to the type of movement, the most represented landslides in the study area are slides (9867 landslides, Fig. 5a) covering a total landslide area of 287 km^2. The 4657 slide-earth flows (Fig. 5b) cover an area of 158 km^2, whereas earth flows are represented by 2435 landslides (Fig. 5c) covering an area of 46 km^2. Table 2 reveals that these three classes represent more than 95 % of the total landslides, while debris flows (38), rockfalls (1), and sackungs (1) are rare.

The main features of the three more represented landslide types are illustrated in Fig. 6. Inspection of the figure highlights the main cartographic differences (Fig. 6a, c, e) between the different landslide types (Fig. 6b, d, f).

Figure 6a, b illustrate the slide-type landslides. Such failures present a well-defined scarp which can be semi-circular (rotational slides) or angular (translational slides). The slide deposit is convex, with a morphologically depressed head of the deposit characterised by a centripetal drainage and local counter-slopes and a toe characterised by a typical upward bulge (Fig. 6b). It is reasonable to expect a volume balancing between escarpment and deposit areas since slides are usually characterised by low mobility of landslide material. This is clear in Fig. 6a, b, which shows a planimetric and altimetric shift of about 25 m of the displaced material, with no evidence of chaotic rearrangement and/or volumetric changes.

Slide-earth flows (Fig. 6c, d) start as slides and then evolve into flows. Therefore, they show the characteristics of slides (most commonly rotational) in the escarpment area and in the head of the deposit, where local endorheic conditions can promote seasonal swamps with diffuse organic soil development (Fig. 6c, d). On the other hand, the transport zone and accumulation zone are more similar to earth flows, characterised by the typical lobe shape of the accumulation zone (Fig. 6c, d).

Earth flows (Fig. 6e, f) are characterised by an overall elongated planar shape, with the median part narrower than the detachment and accumulation zones. The mobility of earth flows is generally higher than slides, which is also evident in their more elongated shape. A typical earth flow is usually bounded by lateral streams draining the deposits into the main river valley, which typically experiences narrowing of the valley section and erosion on the opposite side of the landslide toe (Fig. 6f).

Debris flows and rockfalls are not statistically represented in our inventory because the Daunia Apennines lack the environmental conditions favouring their development, such as steep rocky slopes and sub-vertical cliffs. However, local geomorphological conditions (e.g. steep edges of suspended fluvial terraces) can promote the formation of coalescing phenomena of small debris flows and small rockfalls, which cannot be mapped individually but which were included within areas with widespread landslides (Fig. 5d,

Table 2. Descriptive statistics of landslides by type.

Landslide type	Number of features	Total area (m^2)	Minimum area (m^2)	Maximum area (m^2)
Slide type	9867	2.9×10^8	1.9×10^1	6.8×10^6
Earth flow	2435	4.6×10^7	3.6×10^1	1.3×10^7
Slide-earth flow	4657	1.6×10^8	8.8×10^1	2.9×10^6
Debris flow	38	6.5×10^5	1.4×10^2	1.4×10^5
Rockfall	1	6.0×10^4	6.0×10^4	6.0×10^4
Sackung	1	5.0×10^5	5.0×10^5	5.0×10^5
Total	16 999	4.3×10^8	1.9×10^1	1.3×10^7
Widespread landslide	Number of features	Total area (m^2)	Minimum area (m^2)	Maximum area (m^2)
Shallow earth/soil slides and earth flows	138	7.1×10^6	5.2×10^2	3.5×10^5
Debris flow	193	4.1×10^6	3.8×10^2	1.4×10^5
Rockfall	17	1.3×10^5	5.2×10^2	2.4×10^4
Total	348	1.1×10^7	3.8×10^2	3.5×10^5
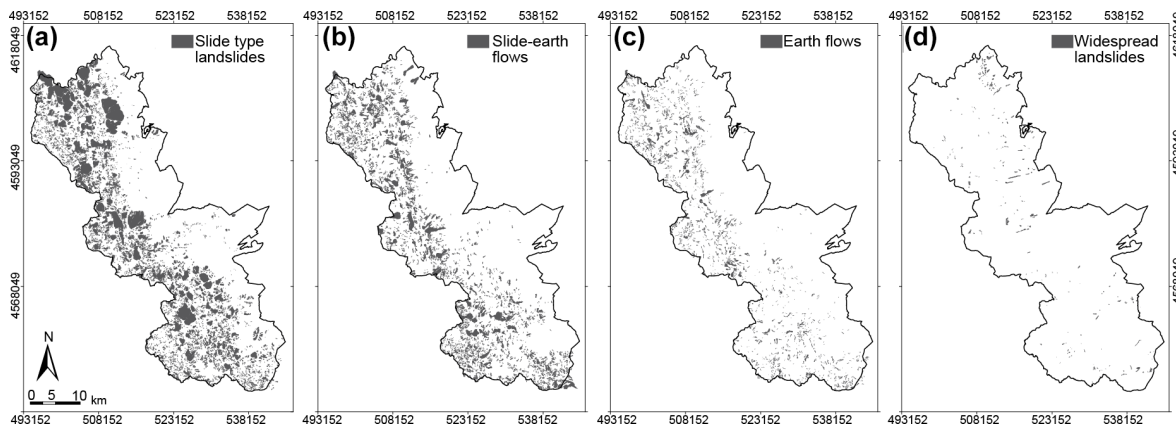
Figure 5. Spatial distribution of **(a)** slide-type landslides, **(b)** slide-earth flows, **(c)** earth flows, and **(d)** widespread landslides.

Sect. 4.4). Finally, sackungs are poorly represented in our study area.

4.3 Landslide estimated depth

The estimated depth of a landslide is assigned based on the main morphological characteristics of the landslide, such as slope height, and the extent of curvatures along the slope (convexity and concavity). Based on these morphological characteristics, landslides were classified as deep-seated or shallow.

Deep-seated landslides are predominantly represented by failures that cover considerable extents, even exceeding 1 km^2. Many of the deep-seated landslides can be classified as very old relict, very old, and old. They often involve considerable volumes of material and can alter the local morphology and geological structure. In the inventory map, deep-seated landslides are represented with two polygons, distinguishing the deposit area from the scarp area.

Shallow landslides are generally small ($\sim 10^4$ m^2) and mainly represented by slide-type and flow-type landslides. They are generally characterised by a not very pronounced scarp, with an estimated height of less than 2 m, and by a deposit without evident concavities and convexities on its surface. In the inventory, shallow landslides are mapped as single polygons, including both the scarp and the deposit area.

4.4 Widespread landslides

The areas of widespread landslides (Table 2, Fig. 5d) are represented by landslides whose sizes are smaller than the smallest feature that can be represented at the publication scale of the final map. In the map we distinguished between (i) shallow earth/soil slides and earth flows, (ii) debris
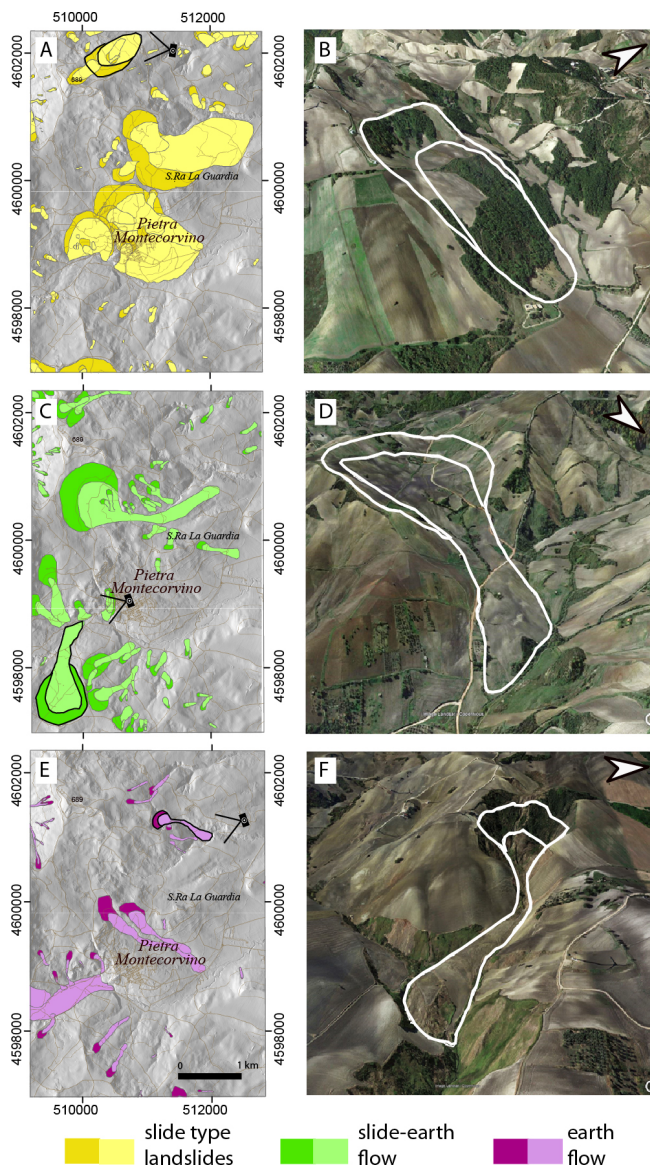
Figure 6. Examples on the map (**a, c, e**) and on © GoogleEarth™. Images (**b, d, f**) of slide-type failures (**a, b**), slide-earthflow landslides (**c, d**), and earthflows (**e, f**). For each row, black-outlined polygons and camera symbols in the left image identify the landslide shown in the corresponding image on the right and the point of view, respectively.

flows, and (iii) rockfalls. Their spatial distribution is mainly related to locally steep slopes, for instance in the vicinity of badlands, in the crown areas of pre-existing large landslides, or along the edges of ancient suspended fluvial terraces (Fig. 7). Widespread shallow slides and flows typically involve weathered clayey soils, while widespread debris flows and rockfalls are commonly fed by loose debris or poorly cemented conglomerates and breccias. Finally, it was not possible to assign a well-defined age to widespread

landslides, although their morphological evidence suggests seasonal reactivations.

4.5 Descriptive statistics of the G-LIM

Descriptive statistics of landslide number and size are shown in Fig. 7. Box plots in Fig. 7a, b show the distribution of landslide areas for the landslide classified based on the expected relative age (Fig. 7a) and the type of movement (Fig. 7b).

Inspection of the plot in Fig. 7a confirms that slides, slide-earth flows, and flows are the most represented landslides of the inventory. Among these three classes, the slide-type landslides are characterised by the largest size variability, while the slide-earth flows are on average slightly larger than the others. In the plot of Fig. 7a, landslides (on the left) are separated by areas of widespread landslides (on the right) because the latter are not related to a single feature and cannot be directly compared to single landslides. This is the reason why the areas of widespread landslides are on average larger than the single landslides. In particular, the areas of widespread soil slides and earth flows are larger than the others because they typically involve edges of fluvial terraces characterised by strong lateral continuity.

The plot in Fig. 7b shows the size distribution of the four relative age classes of landslides. The clear separation of the age classes according to their median values is a statistically robust indication of the reliability of this landslide classification strategy, which is under-used in the landslide-oriented international literature.

Comparing Fig. 7a and b, it is worth noting that the median area of all the landslide types is around 10^5 m^2, which corresponds to the median area of the old landslide group. This was expected since this is the most represented landslide age class within the inventory.

Figure 7c shows landslide count (represented by a colour gradient and labels) and cumulated area (proportional to circle sizes), grouped by relative age class and landslide type. Visual inspection of the plot reveals that relict and very old landslides are not represented by small landslides, and in particular by debris flows and rockfalls, which tend to be small and easily obliterated by erosion and subsequent failures. Further evidence is that a large portion of the total landslide area is occupied by few relict and very old kilometre-scale slope failures, whereas a decreasing trend in both cumulated area and the total number of landslides is evident through time for all landslide types within the old landslide age class. Such evidence suggests a size threshold effect of previous landslides on subsequent slope movements, probably controlled by slope-scale morphological and hydrological perturbations induced by the occurrence of the first failure.

4.6 Geomorphological elements

In the landslide inventory map, some geomorphological elements are also reported in addition to the mass movements
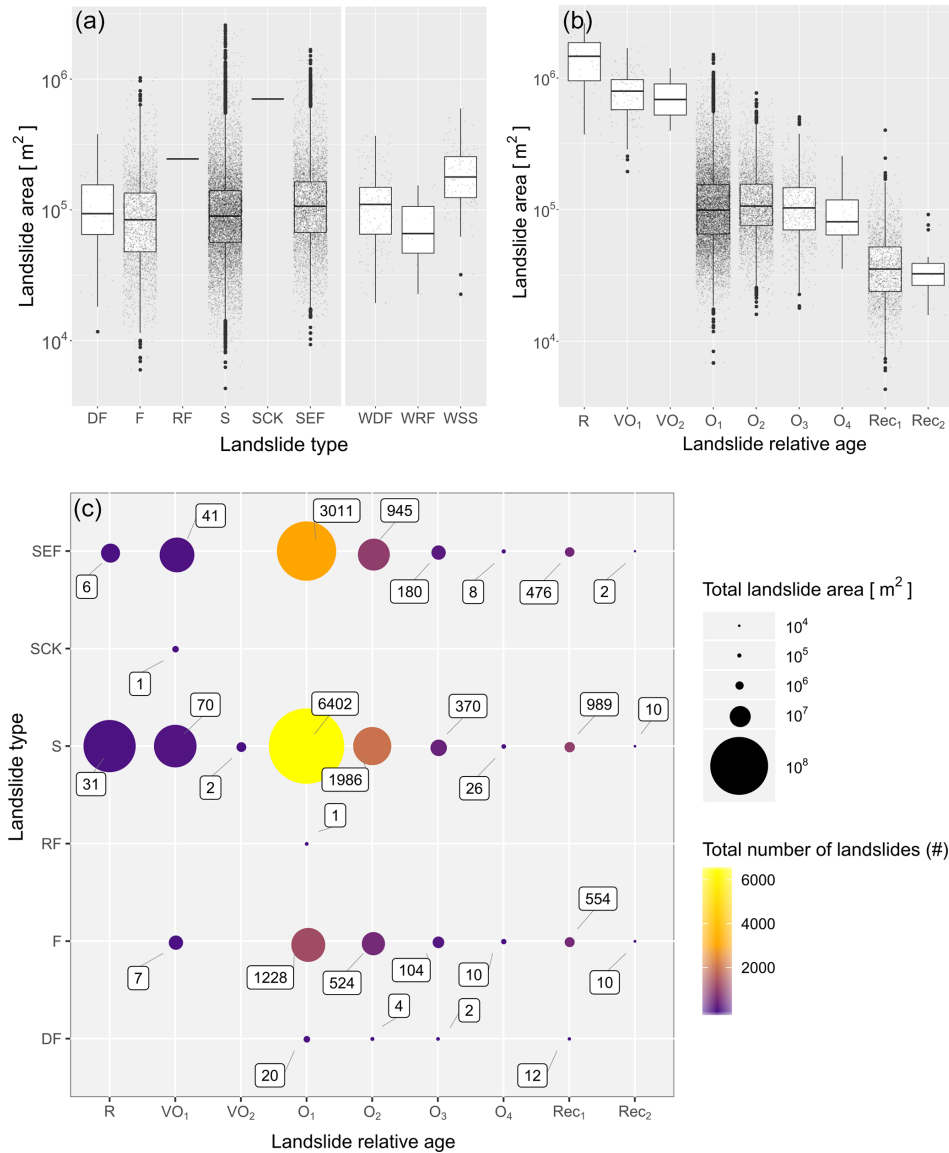
Figure 7. Plots summarising landslide statistics. **(a)** Landslide number (represented by a colour gradient and labels) and cumulated area (proportional to circle sizes), grouped by relative age class and landslide type (SK, sackung; SEF, slide-earth flow; S, slide; RF, rockfall; DF, debris flow; EF, earth flow). **(b)** Distribution of landslide areas within each relative age class. The relative age classes are indicated through a letter (R, relict; V, very old; O, old) and a subscript number that indicates the generation within the age class (1–4). **(c)** Scatterplot showing cumulative sizes and counts of landslides grouped by relative age in the abscissa and type in the ordinate. Landslide number is represented by a colour gradient and labels; total area is proportional to circle sizes.

(Fig. 8). Such elements can be considered in relation to slope evolution and can provide useful information for landslide identification and mapping. In particular, our map includes alluvial deposits, fluvial terraces, and alluvial fans. Alluvial deposits are flat and always located in the lowest portions of the Tavoliere delle Puglie plain and along the main water courses draining the hilly and mountainous areas of the Daunia Apennines. Older alluvial/fluvial deposits are nowadays suspended over the present-day base level and are organised in fluvial terraces at different elevations, recording the ongoing deepening of the drainage network during the Quaternary. Alluvial fans were recognised and mapped into two relative age classes according to their appearance. They were classified as relict if dismantled and dissected due to the incision of the present-day river network. They were instead classified as recent if well preserved.
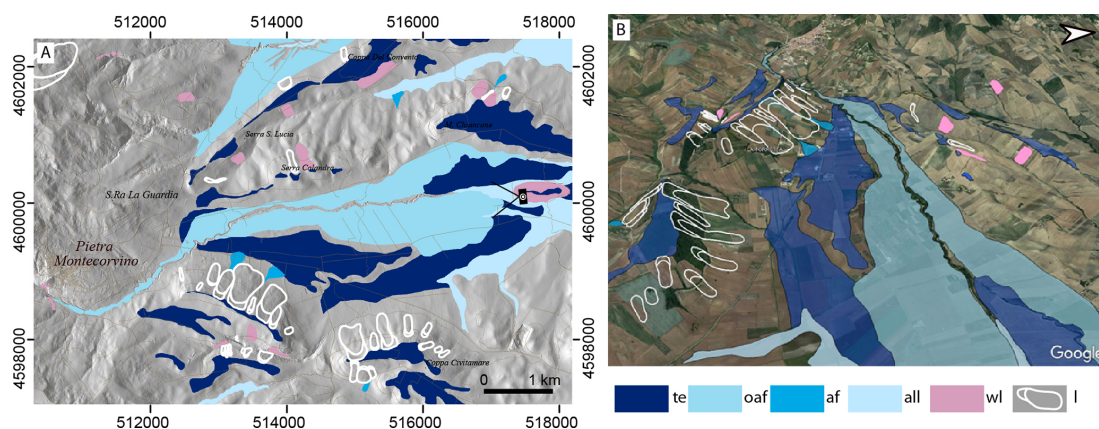
Figure 8. (a) Excerpt of the landslide inventory map. Landslides were coloured in white to enhance the geomorphological elements. **(b)** Birds-eye view of the same area as **(a)** prepared using © GoogleEarth™. In the legend: te, fluvial terrace; oaf, old alluvial fan; af, alluvial fan; all, alluvial deposits; wl, widespread landslide; l, landslide.

5 Data availability

The dataset is available at https://doi.org/10.1594/PANGAEA.942427 (Cardinali et al., 2022).

6 Conclusions

The landslide inventory map presented in this paper is a new catalogue of landslide phenomena in the Daunia Apennines. It provides new data uniformly distributed over the study area at an unprecedented cartographic detail.

The new landslide inventory map was produced upon request of the authorities of the Apulia region to solve the heterogeneity and limitations in the currently available landslide inventories (Pellicani et al., 2014b; Pellicani and Spilotro, 2015), mainly due to (i) partial coverage of the territory, (ii) heterogeneity in the degree of cartographic detail, (iii) lack of metadata and other methodological information, and (iv) geospatial inconsistencies where the different products overlap.

The new inventory represents a significant improvement upon earlier mapping because (i) it presents a new homogeneous landslide coverage for the Daunia Apennines, (ii) it is acquired with a uniform method and based on rigorous and reproducible criteria, (iii) it keeps the same cartographic detail throughout the entire area, and (iv) it presents a systematic classification of landslides by type, relative age, and depth, hence providing basic information at 1 : 5000 scale for landslide characterisation and related land management activities. In addition, the spatially distributed information on landslide coverage portrayed in the map and the detailed scale of mapping provide the fundamental information for landslide susceptibility and hazard assessment (Guzzetti et al., 2005) and for supporting and integrating the study of seismic microzonation and the assessment of seismic hazard in both urban and rural areas (Vignaroli et al., 2019). In addition to the technical and land management benefits, our inventory provides new data to further investigate the Quaternary evolution of the landscape of this part of the southern Apennines.

Analysis of the data revealed that the great majority of landslide volume was mobilised by relict and very old landslides, whereas the landslide maximum size decreased over time and tended to cluster around pre-existing failures. The results have relevance for determining the statistics of landslide size (Malamud et al., 2004) and for triggering detailed studies on the types, patterns, and distributions of landslides in relation to geology (Bucci et al., 2016b), structure (Bucci et al., 2013), and tectonic (Bucci et al., 2014) and climatic forcing (Schiattarella et al., 2017). The presented dataset also documents the relationships between landslides and other geomorphological elements, in particular with ancient and recent alluvial deposits and alluvial fans. These fluvially related landforms can be used as input data to study Quaternary depositional (Mirabella et al., 2018) and erosional events (Mancini et al., 2020) and, in combination with landslide information, to study the interplay of gravitational and fluvial processes (Santangelo et al., 2013).

In the G-LIM presented, the vast majority of landslides are slow-moving, whereas rapid and fast landslides are rare (debris flows and rockfalls). Such evidence should be further confirmed by in-depth studies (e.g. multi-temporal inventories or susceptibility models) as it may indicate a relatively low exposure of human life compared to other mountain areas of the southern Apennines. On the other hand, it must be taken into account that the increasing frequency of extreme rainfall events may also trigger rapid- and fast-moving landslides in this area, differently from what was observed in the past. This aspect further shows that systematic landslide mapping to prepare new inventories and update the existing ones is crucial, particularly in the ongoing climate change scenario.

We acknowledge that scarcity of data represents a limitation and a challenge for the landslide community. Most regional-scale studies are less effective (or analysed) than expected due to the lack of easy sharing of landslide information in digital format. Our work is also intended as a contribution to the broader geomorphological community, promoting the sharing of a landslide dataset at regional scale from various environments.

Finally, it is worth remembering that a landslide map, even if accurate, does not answer all questions regarding hazards or risk at any scale. A landslide map is informative about the area covered by landslides, but nothing can be said about the remaining territory. The map dataset should be used as an indication to optimise resources and to plan investigations aimed at determining landslide hazard and risk at a larger scale. In our case, the map dataset is published at the 1 : 5000 scale and should be consulted at most at the same level of detail.

Appendix A

In the first phase of the work, information and cartographic/thematic products were collected to support the preparation of the geomorphological landslide inventory map of the Daunia Apennines. Some of the listed products have been provided by Regione Puglia and others can be consulted on the web through cartographic portals or web servers.

- Regional technical maps in digital format at scale 1 : 5000 supplied by Regione Puglia (https://www.sit.puglia.it)

- Geological maps at scale 1 : 50 000 (CARG, CARtografia Geologica) available on the Istituto Superiore per la Protezione e la Ricerca Ambientale (ISPRA) cartographic portal

- Geological maps at scale 1 : 100 000 (Geological Map of Italy) available on the ISPRA cartographic portal

- Hydrogeomorphological map at scale 1 : 25 000 available on the SIT site of Regione Puglia (http://webapps.sit.puglia.it/freewebapps/Idrogeomorfologia/index.html, last access: 6 February 2023)

- Digital elevation model (DEM, cell 8×8 m) provided by Regione Puglia (https://www.sit.puglia.it)

- DEM made by lidar (1×1 m cell), carried out within the framework of the Extraordinary Plan for Environmental Remote Sensing (PST-A) and provided by the Ministry of Ecological Transition (MiTE)

- Urbanised and land use maps provided by Regione Puglia (https://www.sit.puglia.it)

- Orthophoto maps provided by Regione Puglia (https://www.sit.puglia.it)

- Landslide inventory maps of Apulia from the following:

  - *IFFI Inventory*. Inventory of Landslide Phenomena in Italy, compiled by ISPRA

  - Official archives: *Piano Stralcio per l'Assetto Idrogeologico* (PAI) of the basin authorities of Puglia and Basilicata, of the Trigno, Biferno, and minor Saccione and Fortore rivers, and of the Liri–Garigliano and Volturno rivers. *Project Inventory of Franosi Phenomena in Italy (IFFI – update 2006)*, compiled by ISPRA. *Census Project of Italian Areas Historically Vulnerable to Geological and Hydraulic Disasters (AVI)*, drawn up by the National Group for Defence against geohydrological Disasters of the National Research Council (GNDCI-CNR)

  - AdBP photo interpretation: landslides from the photo interpretation study conducted by AdBP (Basin Authority of the Apulia region)

  - Province of Foggia: this deals with the landslides surveyed by the Province of Foggia within the framework of the agreements signed with the AdBP concerning the "Activity of collection and classification of data on landslide phenomena in the Province of Foggia" and "Conduct of studies for the deepening of the aspects related to the classified landslide phenomena".

References

Antonini, G., Ardizzone, F., Cardinali, M., Galli, M., Guzzetti, F., and Reichenbach, P.: Surface deposits and landslide inventory map of the area affected by the 1997 Umbria-Marche earthquakes, Bollettino della Società Geologica Italiana, Volume SPE, 121, 843–853, 2002.

Ardizzone, F., Basile, G., Cardinali, M., Casagli, N., Del Conte, S., Del Ventisette, C., Fiorucci, F., Garfagnoli, F., Gigli, G., Guzzetti, F., Iovine, G., Mondini, A. C., Moretti, S., Panebianco, M., Raspini, F., Reichenbach, P., Rossi, M., Tanteri, L., and Terranova, O.: Landslide inventory map for the Briga and the Giampilieri catchments, NE Sicily, Italy, J. Maps, 8, 176–180, https://doi.org/10.1080/17445647.2012.694271, 2012.

Ardizzone, F., Fiorucci, F., Santangelo, M., Cardinali, M., Mondini, A. C., Rossi, M., Reichenbach, P., Guzzetti, F., and Ardizzone, F.: Very-High Resolution Stereoscopic Satellite Images for Landslide Mapping, in: Landslide Inventory and Susceptibility and Hazard Zoning, Berlin, Heidelberg, Citation Key: CNR-PRODOTTI89033, 95–101, 2013.

Brozzetti, F., Boncio, P., Lavecchia, G., and Pace, B.: Present activity and seismogenic potential of a low-angle normal fault system (Città di Castello, Italy): Constraints from surface geology, seismic reflection data and seismicity, Tectonophysics, 463, 31–46, https://doi.org/10.1016/j.tecto.2008.09.023, 2009.

Bucci, F., Cardinali, M., and Guzzetti, F.: Structural geomorphology, active faulting and slope deformations in the epicentre area of the MW 7.0, 1857, Southern Italy earthquake, Phys. Chem. Earth, 63, 12–24, https://doi.org/10.1016/j.pce.2013.04.005, 2013.

Bucci, F., Novellino, R., Tavarnelli, E., Prosser, G., Guzzetti, F., Cardinali, M., Gueguen, E., Guglielmi, P., and Adurno, I.: Frontal collapse during thrust propagation in mountain belts: a case study in the Lucania Apennines, Southern Italy, J. Geol. Soc., 171, 571–581, https://doi.org/10.1144/jgs2013-103, 2014.

Bucci, F., Santangelo, M., Cardinali, M., Fiorucci, F., and Guzzetti, F.: Landslide distribution and size in response to Quaternary fault activity: The Peloritani Range, NE Sicily, Italy, Earth Surf. Proc. Land., 41, 711–720, https://doi.org/10.1002/esp.3898, 2016a.

Bucci, F., Mirabella, F., Santangelo, M., Cardinali, M., and Guzzetti, F.: Photo-geology of the Montefalco Quaternary Basin, Umbria, Central Italy, J. Maps, 12, 314–322, https://doi.org/10.1080/17445647.2016.1210042, 2016b.

Bucci, F., Santangelo, M., Fiorucci, F., Ardizzone, F., Giordan, D., Cignetti, M., Notti, D., Allasia, P., Godone, D., Lagomarsino, D., Pozzoli, A., Norelli, E., and Cardinali, M.: Geomorphologic landslide inventory by air photo interpretation of the High Agri Valley (Southern Italy), J. Maps, 17, 376–388, https://doi.org/10.1080/17445647.2021.1943552, 2021.

Cardinali, M., Antonini, G., Reichenbach, P., and Guzzetti, F.: Photo geological and landslide inventory map for the Upper Tiber River basin. Pubblication CNR GNDCI n. 2116, Scale 1:1,200,000, 2001 (in English and Italian).

Cardinali, M., Ardizzone, F., Bucci, F., Fiorucci, F., Pisano, L., Santangelo, M., and Zumpano, V.: Geomorphological landslide inventory map of the Daunia Mountains, Southern Italian Apennines, PANGAEA [data set], https://doi.org/10.1594/PANGAEA.942427, 2022.

Ciarcia, S., Di Nocera, S., Matano, F., and Torre, Ma. L.: Evoluzione tettono-sedimentaria e paleogeografica dei depocentri "wedge-top" nell'ambito del "foreland basin system" pliocenico dell'Appennino meridionale (settore Irpino-Dauno), Boll. Soc. Geol. It., 122, 117–137, 2003.

Cotecchia, F., Santaloia, F., and Tagarelli, V.: Towards A Geo-Hydro-Mechanical Characterization of Landslide Classes: Preliminary Results, Appl. Sci., 10, 7960, https://doi.org/10.3390/app10227960, 2020.

Cruden, D. M. and Varnes, D. J.: Landslide Types and Processes, Special Report National Research Council Transportation Research Board, 247, 36–75, 1996.

di Lernia, A., Cotecchia, F., Elia, G., Tagarelli, V., Santaloia, F., and Palladino, G.: Assessing the influence of the hydraulic boundary conditions on clay slope stability: The Fontana Monte case study, Eng. Geol., 297, 106509, https://doi.org/10.1016/j.enggeo.2021.106509, 2022.

Donnini, M., Napolitano, E., Salvati, P., Ardizzone, F., Bucci, F., Fiorucci, F., Santangelo, M., Cardinali, M., and Guzzetti, F.: Impact of event landslides on road networks: a statistical analysis of two Italian case studies, Landslides, 14, 1521–1535, https://doi.org/10.1007/s10346-017-0829-4, 2017.

Filice, F. and Seeber, L.: The Culmination of an Oblique Time-Transgressive Arc Continent Collision: The Pollino Massif Between Calabria and the Southern Apennines, Italy, Tectonics, 38, 3261–3280, https://doi.org/10.1029/2017TC004932, 2019.

Fiorucci, F., Ardizzone, F., Rossi, M., and Torri, D.: The Use of Stereoscopic Satellite Images to Map Rills and Ephemeral Gullies, Remote Sensing, 7, 14151–14178, https://doi.org/10.3390/rs71014151, 2015.

Fiorucci, F., Giordan, D., Santangelo, M., Dutto, F., Rossi, M., and Guzzetti, F.: Criteria for the optimal selection of remote sensing optical images to map event landslides, Nat. Hazards Earth Syst. Sci., 18, 405–417, https://doi.org/10.5194/nhess-18-405-2018, 2018.

Froude, M. J. and Petley, D. N.: Global fatal landslide occurrence from 2004 to 2016, Nat. Hazards Earth Syst. Sci., 18, 2161–2181, https://doi.org/10.5194/nhess-18-2161-2018, 2018.

Galli, M., Ardizzone, F., Cardinali, M., Guzzetti, F., and Reichenbach, P.: Comparing landslide inventory maps, Geomorphology, 94, 268–289, https://doi.org/10.1016/j.geomorph.2006.09.023, 2008.

Gioia, D., Di Leo, P., Giano, S. I., and Schiattarella, M.: Chronological constraints on a Holocene landslide in an intermontane basin of the southern Apennines, Italy: Morphological evolution and palaeoclimate implications, Holocene, 21, 263–273, https://doi.org/10.1177/0959683610378879, 2011.

Guzzetti, F., Reichenbach, P., Cardinali, M., Galli, M., and Ardizzone, F.: Probabilistic landslide hazard assessment at the basin scale, Geomorphology, 72, 272–299, https://doi.org/10.1016/j.geomorph.2005.06.002, 2005.

Guzzetti, F., Mondini, A. C., Cardinali, M., Fiorucci, F., Santangelo, M., and Chang, K.-T.: Landslide inventory maps: New tools for an old problem, Earth-Sci. Rev., 112, 42–66, https://doi.org/10.1016/j.earscirev.2012.02.001, 2012.

Harp, E. L. and Jibson, R. W.: Inventory of landslides triggered by the 1994 Northridge, California earthquake, U.S. Geological Survey [data set], https://doi.org/10.5066/F7Z60MKF, 2017.

Hungr, O., Leroueil, S., and Picarelli, L.: The Varnes classification of landslide types, an update, Landslides, 11, 167–194, https://doi.org/10.1007/s10346-013-0436-y, 2014.

Keaton, J. R. and DeGraff, J. V.: Surface observation and geologic mapping, in: Landslides: Investigation and mitigation, edited by: Turner, A. K. and Schuster, R. L., Transportation Research Board Special Report 247, Washington, D.C., National Research Council, 178–230, 1996.

Losacco, N., Bottiglieri, O., Santaloia, F., Vitone, C., and Cotecchia, F.: The Geo-Hydro-Mechanical Properties of a Turbiditic Formation as Internal Factors of Slope Failure Processes, Geosciences, 11, 429, https://doi.org/10.3390/geosciences11100429, 2021.

Malamud, B. D., Turcotte, D. L., Guzzetti, F., and Reichenbach, P.: Landslide inventories and their statistical properties, Earth Surf. Proc. Land., 29, 687–711, https://doi.org/10.1002/esp.1064, 2004.

Mancini, M., Vignaroli, G., Bucci, F., Cardinali, M., Cavinato, G. P., Di salvo, C., Giallini, S., Moscatelli, M., Polpetta, F., Putignano, M. L., Santangelo, M., and Sirianni, P.: New stratigraphic constraints for the Quaternary source-to-sink history of the Amatrice Basin (central Apennines, Italy), Geol. J., 55, 4226–4251, https://doi.org/10.1002/gj.3672, 2020.

Mirabella, F., Bucci, F., Santangelo, M., Cardinali, M., Caielli, G., De Franco, R., Guzzetti, F., and Barchi, M. R.: Alluvial fan shifts and stream captures driven by extensional tectonics in central Italy, J. Geol. Soc., 175, 788–805, https://doi.org/10.1144/jgs2017-138, 2018.

Mondini, A. C., Chang, K., Rossi, M., Marchesini, I., and Guzzetti, F.: Semi-automatic recognition and mapping of event-induced landslides by exploiting multispectral satellite images and DEM in a Bayesian framework, SPIE Asia-Pacific Remote Sensing, 2012, Kyoto, Japan, P. SPIE, 852415, https://doi.org/10.1117/12.977432, 2012.

Niculiţă, M., Mărgărint, M. C. M. C., and Santangelo, M.: Archaeological evidence for Holocene landslide activity in the Eastern Carpathian lowland, Quatern. Int., 415, 175–189, https://doi.org/10.1016/j.quaint.2015.12.048, 2016.

Pánek, T., Hartvich, F., Jankovská, V., Klimeš, J., Tábořík, P., Bubík, M., Smolková, V., and Hradecký, J.: Large Late Pleistocene landslides from the marginal slope of the Flysch Carpathians, Landslides, 11, 981–992, https://doi.org/10.1007/s10346-013-0463-8, 2014.

Pellicani, R. and Spilotro, G.: Evaluating the quality of landslide inventory maps: comparison between archive and surveyed inventories for the Daunia region (Apulia, Southern Italy), Bull. Eng. Geol. Environ., 74, 357–367, https://doi.org/10.1007/s10064-014-0639-z, 2015.

Pellicani, R., Van Westen, C. J., and Spilotro, G.: Assessing landslide exposure in areas with limited landslide information, Landslides, 11, 463–480, https://doi.org/10.1007/s10346-013-0386-4, 2014a.

Pellicani, R., Frattini, P., and Spilotro, G.: Landslide susceptibility assessment in Apulian Southern Apennine: heuristic vs. statistical methods, Environ. Earth Sci., 72, 1097–1108, https://doi.org/10.1007/s12665-013-3026-3, 2014b.

Petley, D.: Global patterns of loss of life from landslides, Geology, 40, 927–930, https://doi.org/10.1130/G33217.1, 2012.

Razak, K. A., Santangelo, M., Westen, C. J. V., Straatsma, M. W., and Jong, S. M. D.: Generating an optimal DTM from airborne laser scanning data for landslide mapping in a tropical forest environment, Geomorphology, 190, 112–125, https://doi.org/10.1016/j.geomorph.2013.02.021, 2013.

Santangelo, M., Gioia, D., Cardinali, M., Guzzetti, F., and Schiattarella, M.: Interplay between mass movement and fluvial network organization: An example from southern Apennines, Italy, Geomorphology, 188, 54–67, https://doi.org/10.1016/j.geomorph.2012.12.008, 2013.

Santangelo, M., Gioia, D., Cardinali, M., Guzzetti, F., and Schiattarella, M.: Landslide inventory map of the upper Sinni River valley, Southern Italy, J. Maps, 11, 444–453, https://doi.org/10.1080/17445647.2014.949313, 2015.

Santangelo, M., Cardinali, M., Bucci, F., Fiorucci, F., and Mondini, A. C.: Exploring event landslide mapping using Sentinel-1 SAR backscatter products, Geomorphology, 397, 108021, https://doi.org/10.1016/j.geomorph.2021.108021, 2022.

Schiattarella, M., Di Leo, P., Beneduce, P., and Ivo Giano, S.: Quaternary uplift vs tectonic loading: a case study from the Lucanian Apennine, southern Italy, Quatern. Int., 101–102, 239–251, https://doi.org/10.1016/S1040-6182(02)00126-X, 2003.

Schiattarella, M., Giano, S. I., and Gioia, D.: Long-term geomorphological evolution of the axial zone of the Campania-Lucania Apennine, southern Italy: a review, Geol. Carpath., 68, 57–67, https://doi.org/10.1515/geoca-2017-0005, 2017.

Schulz, W. H.: OF-2004-1396: Landslides mapped using LIDAR imagery, Seattle, Washington, U.S. Geological Survey, 2004.

Spalluto, L., Fiore, A., Miccoli, M. N., and Parise, M.: Activity maps of multi-source mudslides from the Daunia Apennines (Apulia, southern Italy), Nat. Hazards, 106, 277–301, https://doi.org/10.1007/s11069-020-04461-3, 2021.

Thiery, Y., Terrier, M., Colas, B., Fressard, M., Maquaire, O., Grandjean, G., and Gourdier, S.: Improvement of landslide hazard assessments for regulatory zoning in France: STATE–OF–THE-ART perspectives and considerations, Int. J. Disast. Risk Re., 47, 101562, https://doi.org/10.1016/j.ijdrr.2020.101562, 2020.

Van Den Eeckhaut, M., Poesen, J., Verstraeten, G., Vanacker, V., Nyssen, J., Moeyersons, J., Beek, L. P. H. van, and Vandekerckhove, L.: Use of LIDAR-derived images for mapping old landslides under forest, Earth Surf. Proc. Land., 32, 754–769, https://doi.org/10.1002/esp.1417, 2007.

Vignaroli, G., Mancini, M., Bucci, F., Cardinali, M., Cavinato, G. P., Moscatelli, M., Putignano, M. L., Sirianni, P., Santangelo, M., Ardizzone, F., Cosentino, G., Di Salvo, C., Fiorucci, F., Gaudiosi, I., Giallini, S., Messina, P., Peronace, E., Polpetta, F., Reichenbach, P., Scionti, V., Simionato, M., and Stigliano, F.: Geology of the central part of the Amatrice Basin (Central Apennines, Italy), J. Maps, 15, 193–202, https://doi.org/10.1080/17445647.2019.1570877, 2019.

Vitale, S. and Ciarcia, S.: Tectono-stratigraphic and kinematic evolution of the southern Apennines/Calabria–Peloritani Terrane system (Italy), Tectonophysics, 583, 164–182, https://doi.org/10.1016/j.tecto.2012.11.004, 2013.

Vitale, S., Ciarcia, S., Mazzoli, S., and Zaghloul, M. N.: Tectonic evolution of the "Liguride" accretionary wedge in the Cilento area, southern Italy: A record of early Apennine geodynamics, J.

Geodyn., 51, 25–36, https://doi.org/10.1016/j.jog.2010.06.002, 2011.

Wasowski, J., Lamanna, C., and Casarano, D.: Influence of land-use change and precipitation patterns on landslide activity in the Daunia Apennines, Italy, Q. J. Eng. Geol. Hydroge., 43, 387–401, https://doi.org/10.1144/1470-9236/08-101, 2010.

Wasowski, J., Lamanna, C., Gigante, G., and Casarano, D.: High resolution satellite imagery analysis for inferring surface–subsurface water relationships in unstable slopes, Remote Sens. Environ., 124, 135–148, https://doi.org/10.1016/j.rse.2012.05.007, 2012.

WP/WLI: International Geotechnical societies UNESCO Working Party on World Landslide Inventory, Multilingual landslide glossary, Richmond: A suggested method for desciling the activity of a landslide, Bulletin International Association of Engineering Geology, 47, 53–57, 1993.

Zumpano, V., Ardizzone, F., Bucci, F., Cardinali, M., Fiorucci, F., Parise, M., Pisano, L., Reichenbach, P., Santaloia, F., Santangelo, M., Wasowski, J., and Lollino, P.: The relation of spatio-temporal distribution of landslides to urban development (a case study from the Apulia region, Southern Italy), J. Maps, 17, 133–140, https://doi.org/10.1080/17445647.2020.1746417, 2020.